all along the manipulated area, would be representative of the rib geometry for given test conditions. The explored Mach numbers and stagnation pressure ranges allowed variations of the $\overline{h_w^+}$ parameter from 2 to 31.

Computations based on the integral method showed that the friction contribution of the manipulated area was almost independent of the freestream conditions and equal to 65% of the total drag of the model. The variations of the friction drag coefficient of the manipulated area are plotted vs $\overline{h_w^+}$ in Fig. 3, taken from Walsh and Anders.[9] Such a representation allows us to gather together the results, even though some scatter is observed; the latter is not due to the Mach number but could be attributed to the extreme sensitivity of drag decreases to cross section uniformity, surface finition, etc.

Hence, these supersonic results are compared with Gaudet's data and both the low-speed film data and the fit of transonic data. It should be noted that for $\overline{h_w^+} < 20$, drag decreases are obtained while increases are recorded for higher values; maximum friction drag reductions occur for $\overline{h_w^+}$ close to 10. The drag reducing benefits are comparable to those recorded earlier by several investigators at different speeds. Thus, our supersonic data fit perfectly with the other data, provided that the rib height is scaled with the variables taken at the wall.

Acknowledgments

The authors wish to acknowledge the "Service Technique des Programmes Aéronautiques" for supporting this study and 3M-France for providing the riblet material. They are also grateful to the whole team from the ONERA/Modane-Avrieux S2 wind tunnel.

References

[1]Walsh, M. J., "Riblets," *Viscous Drag Reduction in Boundary Layers*, edited by D. M. Bushnell and J. N. Hefner, Progress in Astronautics and Aeronautics, AIAA, Washington, DC, 1990, pp. 203–261.

[2]Savill, A. M., "Drag Reduction by Passive Devices: A Review of Some Recent Developments," *Structure of Turbulence and Drag Reduction*, edited by A. Gyr, International Union of Theoretical and Applied Mechanics Symposium (Zürich, Switzerland), Springer-Verlag, Berlin, 1990, pp. 429–465.

[3]Coustols, E., and Savill, A. M., "Turbulent Skin Friction Drag Reduction by Active and Passive Means," AGARD Rept. 786, 1992.

[4]Coustols, E., "Behaviour of Internal Manipulators: Riblet Models in Subsonic and Transonic Flows," AIAA Paper 89-0963, March 1989.

[5]Coustols, E., and Cousteix, J., "Experimental Investigation of Turbulent Boundary Layers Manipulated with Internal Devices: Riblets," *Structure of Turbulence and Drag Reduction*, edited by A. Gyr, International Union of Theoretical and Applied Mechanics Symposium (Zürich, Switzerland), Springer-Verlag, Berlin, 1990, pp. 577–584.

[6]Coustols, E., and Cousteix, J., "Experimental Manipulation of Turbulent Boundary Layers in Zero Pressure Gradient Flows Through External and Internal Devices," *Proceedings of the Seventh Symposium on Turbulent Shear Flows* (Stanford, CA), Vol. 2, 1989, Paper 25-3.

[7]Coustols, E., and Schmitt, V., "Synthesis of Experimental Riblet Studies in Transonic Conditions," *Turbulence Control by Passive Means*, Fluid Mechanics and its Applications, edited by E. Coustols, Kluwer, Dordrecht, The Netherlands, 1990, pp. 123–140.

[8]Robert, J. P., "Drag Reduction: An Industrial Challenge," AGARD Rept. 786, 1992.

[9]Walsh, M. J., and Anders, J. B, Jr., "Riblet/LEBU Research at NASA Langley," *Applied Scientific Research*, Vol. 46, No. 3, 1989, pp. 255–262.

[10]Benhalilou, M., Anselmet, F., Liandrat, J., and Fulachier, L., "Experimental and Numerical Investigation of a Turbulent Boundary Layer over Riblets," *Proceedings of the Eighth Symposium on Turbulent Shear Flows* (Munich, Germany), Vol. 1, 1991, Paper 18-5.

[11]Choi, H., Moin, P., and Kim, J., "Direct Numerical Simulation of Turbulent Flow over Riblets," Stanford Univ. CTR Manuscript 137, Stanford, CA, July 1992.

[12]Poisson-Quinton, Ph., "A French Look at the Future Supersonic Transport," International Aerospace Symposium, Nagoya, Japan, 1992, ONERA TP 1992-209.

[13]Bushnell, D.M., "Supersonic Aircraft Drag Reduction," *Proceedings of the AIAA 21st Fluid Dynamics, Plasmadynamics and Lasers Conference* (Seattle, WA), AIAA, Washington, DC, June 1990.

[14]Squire, L. C., and Savill, A. M., "Some Experiences of Riblets at Transonic Speeds," *Proceedings of the Turbulent Drag Reduction by Passive Means Conference* (London), Vol. 2, Sept. 1987, pp. 392–407.

[15]Robinson, S. K., "Effects of Riblets on Turbulence in a Supersonic Boundary Layer," AIAA Paper 88-2526, June 1988.

[16]Gaudet, L., "Properties of Riblets at Supersonic Speeds," *Applied Scientific Research*, Vol. 46, No. 3, 1989, pp. 245–254.

Vortex Breakdown over Delta Wings in Unsteady Freestream

Ismet Gursul*
University of Cincinnati, Cincinnati, Ohio 45221
and
Chih-Ming Ho†
University of California, Los Angeles, Los Angeles, California 90024

Introduction

VORTEX breakdown is an intriguing phenomenon that has been observed both on delta wings and in tubes. Compared with the internal flows in tubes, the major difference of the leading-edge vortex over a delta wing is the continuous feeding of vorticity from the leading edge. In the early studies of vortex breakdown over steady delta wings, flow visualization was used extensively to observe the effects of geometric parameters such as angle of attack, sweep, and yaw angle.[1,2] For a summary of observations and related interpretations, the reader is referred to the reviews of Wedemeyer,[3] Lee and Ho,[4] and Rockwell.[5] The observations in tube experiments and different explanations of the phenomena based on instability, wave propagation, and flow stagnation are summarized in several review articles.[6–8]

The observations over steady delta wings and in tubes showed that there are two important parameters affecting vortex breakdown location: *swirl angle* [$\phi = \tan^{-1}(v/u)$, where v and u are the swirl and axial components of velocity, respectively] and *external pressure gradient* outside the vortex core. An increase in the swirl angle or in the magnitude of adverse pressure gradient causes the breakdown location to move upstream. For a leading-edge vortex, the swirl angle is related to the wing geometry such as angle of attack and sweep angle. It was shown that an increase in angle of attack or aspect ratio corresponds to an increase in swirl angle.[4] The streamwise pressure gradient on the suction surface of the wing is an adverse one due to the existence of a trailing edge, and its magnitude depends on angle of attack and sweep angle. For unsteady wings, both the swirl angle and the pressure gradient are expected to vary in time during a maneuver.

In this study, vortex breakdown characteristics over stationary delta wings in an unsteady freestream were investigated. Breakdown may occur over the wing with increasing unsteadiness even when no breakdown is observed over the wing in steady freestream at the same angle of attack. Experiments were conducted on two delta wings (aspect ratio $A = 1$ and 2). The characteristics of breakdown and its time-dependent behavior were documented by flow visualization and laser Doppler anemometer (LDA) measurements.

Experimental Facility

Experiments were conducted in a vertical unsteady water channel with a cross-sectional area of 45.7 × 45.7 cm. The freestream

Presented as Paper 93-0555 at the AIAA 31st Aerospace Sciences Meeting, Reno, NV, Jan. 11–14, 1993; received Jan. 14, 1993; revision received Sept. 9, 1993; accepted for publication Sept. 13, 1993.

*Assistant Professor, Department of Mechanical, Industrial, and Nuclear Engineering. Member AIAA.

†Professor, Mechanical, Aerospace, and Nuclear Engineering Department. Member AIAA.

velocity control was achieved by a rotating gate located downstream of the test section. The principle and the process of controlling the freestream velocity are explained in detail elsewhere.[9] Amplitude and frequency of the freestream speed can be varied over a wide range. The accelerating or decelerating freestream can also be obtained in this facility. For the periodic unsteady freestream, the velocity can be represented in the form of

$$U/U_\infty = 1 + R\cos\omega t = 1 + R\cos 2\pi t/T \qquad (1)$$

where U_∞ is the time-averaged velocity, R is the dimensionless amplitude ($R < 1$), and $\omega = 2\pi/T$ is the radial frequency.

The velocity field was measured with a two-component laser Doppler anemometer operated in the forward-scattering mode. The optical system was equipped with a beam expander, a 310-mm focusing lens, and a Bragg cell for frequency shifting. The nominal measuring volume was estimated to be about 0.1 mm in diameter and 1 mm in length. Velocity measurements across the vortex core were made with a spacing as small as $\Delta y = 1$ mm. These measurements were repeated at different streamwise locations spaced as $\Delta x = 1$ cm ($\Delta x/c = 0.036$), covering a domain roughly a half-chord length from the trailing edge. The ensemble-averaging technique was applied to the signals to extract deterministic parts.

Different delta wings were used for flow visualization and LDA measurements. For flow visualization, the chord lengths were $c = 20$ cm for $A = 1$ and $c = 17$ cm for $A = 2$. The blockage ratio was 0.044 at the maximum angle of attack $\alpha = 40$ deg. For LDA measurements, a wing with aspect ratio $A = 1$ and $c = 28$ cm was used. At the maximum angle of attack of $\alpha = 28$ deg, the blockage ratio was 0.04. The leading edges of the wings were beveled with a 30-deg angle. The Reynolds number was in the range of 3×10^4 to 6×10^4 for all wings. The freestream turbulence level was about 0.5%. Additional information on experimental techniques can be found in Ref. 10.

Results

The global feature of the vortex breakdown phenomenon in the time-varying freestream was first examined by the flow visualization technique. For a constant value of the reduced frequency $k = \omega c/2U_\infty$ and the amplitude R, the variation of the vortex breakdown position depends on the aspect ratio and angle of attack of the wing (Fig. 1). At a small angle of attack, the vortex breakdown takes place near the trailing edge and moves upstream with an increasing angle of attack. The breakdown position does not change very much during the cycle of freestream velocity variation at a large angle of attack. However, the variations of the vortex breakdown location are fairly large at a small angle of attack. Especially, at a certain phase ($t/T \approx 0.85$), the vortex breakdown

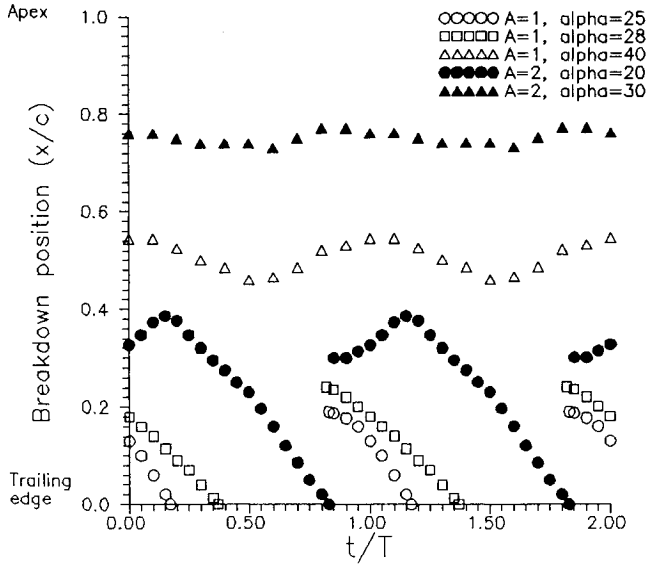

Fig. 1 Variation of vortex breakdown position for sinusoidal freestream variations ($k = 0.93$, $R = 0.42$).

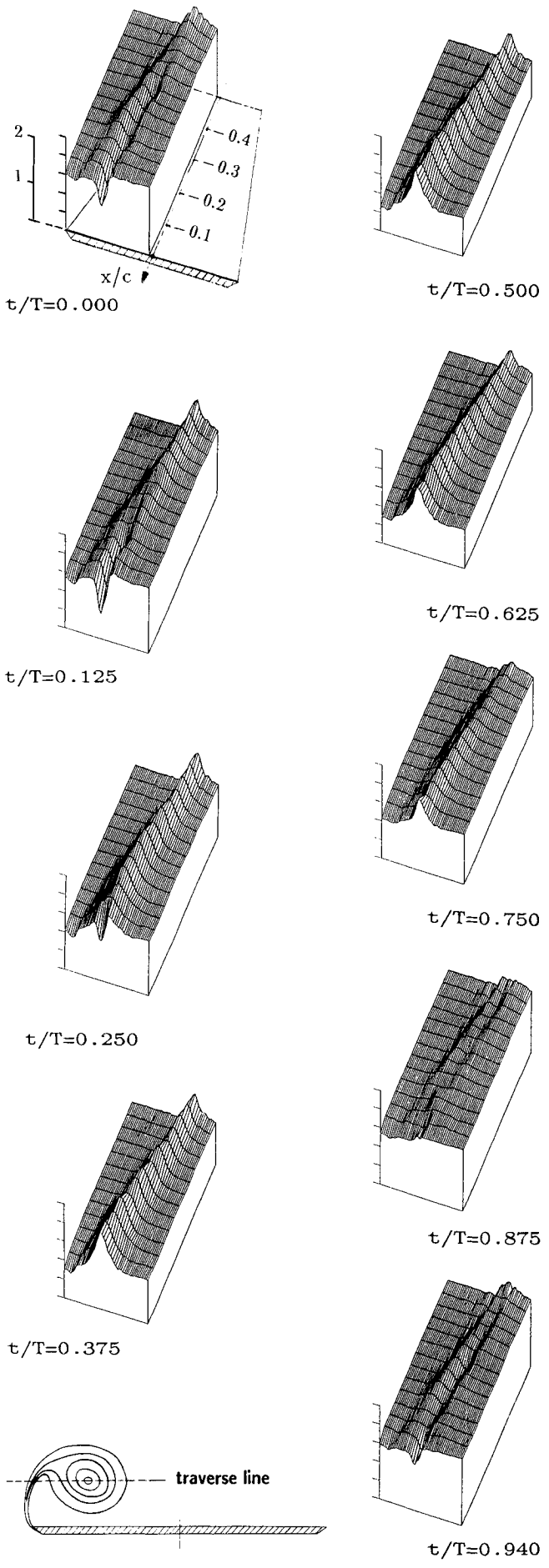

Fig. 2 Normalized axial velocity across the core at different phases of the cycle: $\alpha = 15$ deg, $A = 1$, $k = 1.27$, $R = 0.42$.

suddenly occurs at an upstream location, and then it moves downstream with a convection velocity $U_c \approx 0.2U_\infty$.

The detailed velocity field was measured by LDA for a delta wing with an aspect ratio of unity, $A = 1$. Measurements of velocity components parallel and normal to the wing surface were taken in the plane containing the vortex core axis (see the insert in Fig. 2). Since the measurements were taken along a traverse line parallel to the trailing edge (which is not perpendicular to the vortex axis), the velocity components approximately correspond to the axial and swirl velocities across the vortex core. From phase-averaged measurements taken at different streamwise stations, the velocity field along the vortex core was constructed and presented in Fig. 2 for $\alpha = 15$ deg. (The origin of the coordinate system is located at the trailing edge). When vortex breakdown occurs over the wing, the axial velocity distribution (normalized by U_∞) shows an abrupt transition from a jetlike to a wakelike profile at the breakdown location. During the deceleration ($0 \le t/T \le 0.5$), the breakdown moves downstream. After the breakdown leaves the wing, a jetlike velocity profile is observed everywhere. The acceleration starts at $t/T = 0.5$; however, as the freestream increases, there is not a corresponding increase in the axial velocity inside the vortex core. Around $t/T = 0.75$, the velocity inside the vortex core starts to decrease as the velocity outside the core increases with the freestream. A very interesting feature is observed at $t/T = 0.875$: the velocity is almost uniform everywhere on the wing. After this moment, a wakelike profile is observed from the midchord to the trailing edge. The same phenomenon was observed when the angle of attack is 28 deg (see Ref. 10).

Based on the measured axial and swirl velocity components, the swirl angle can be calculated at each location at every instant. The variation of swirl angle with the distance from the vortex axis was given in detail in Ref. 10. The swirl angle is zero at the center of the vortex core and reaches a maximum at the edge of the subcore; the subcore being the region where most of the streamwise vorticity is confined. The maximum swirl angle does not change much before and after the breakdown. When the maximum swirl angle is plotted as a function of the streamwise distance and time (Fig. 3), this quantity remains constant. The solid line in the x-t plane denotes the movement of the breakdown. At any point downstream of the solid line, a wakelike velocity profile exists. In the shaded time interval, the transition from a jetlike to a wakelike profile takes place. It is concluded that the maximum swirl angle is not correlated with the movement of the vortex breakdown. This suggests that the time-dependent character of the breakdown must be due to other dynamic features.

Hall[6] suggested that vortex breakdown occurs as a result of an adverse pressure gradient along the vortex axis, which leads to a stagnation point. With the assumption of quasicylindrical flow (which is a reasonable approximation before the breakdown),

$$\frac{\partial p}{\partial x}(x, r = 0) = \frac{\partial p}{\partial x}(x, r = R) - \int_0^R \frac{\partial}{\partial x}\left(\frac{\rho v^2}{r}\right) dr \qquad (2)$$

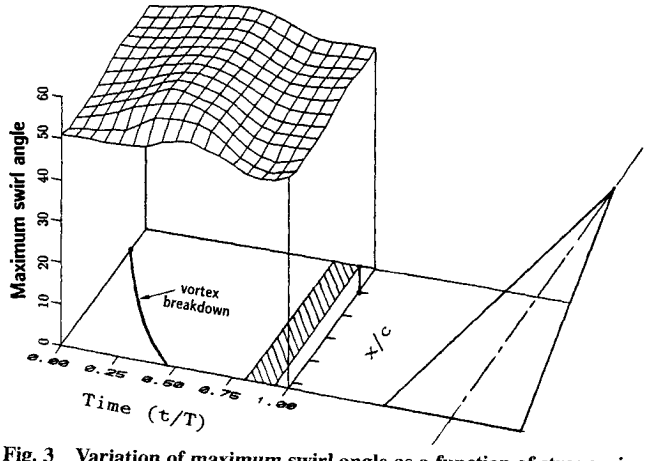

Fig. 3 Variation of maximum swirl angle as a function of streamwise distance and time: $\alpha = 28$ deg, $A = 1$, $k = 1.27$, $R = 0.42$.

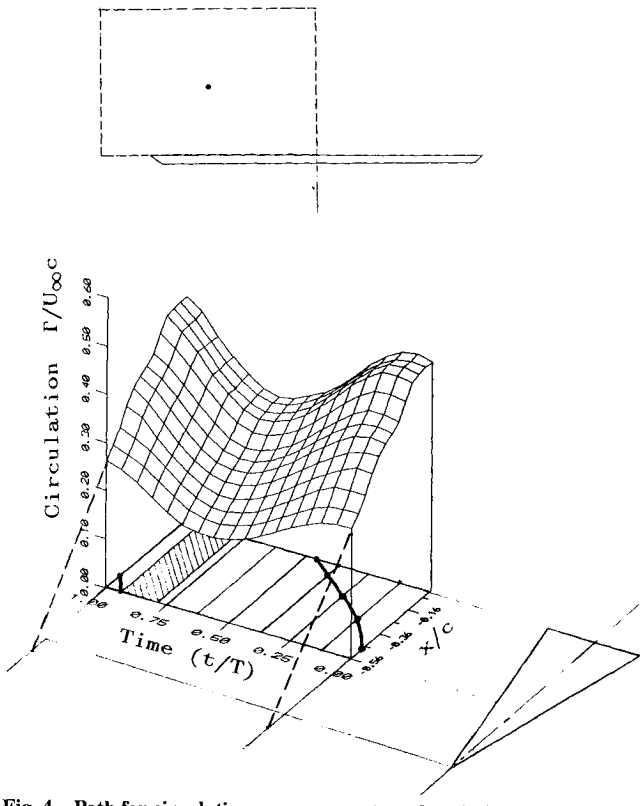

Fig. 4 Path for circulation measurements and variation of dimensionless circulation as a function of streamwise distance and time: $\alpha = 28$ deg, $A = 1$, $k = 1.27$, $R = 0.42$.

In this equation, x is the streamwise distance, r is the radius measured from the center of the vortex, and R is the edge of the vortex where the external boundary conditions exist. The first term is the external pressure gradient, and second term is the contribution due to the swirl component. The latter is related to the swirl angle, which confirms the observations in steady freestream that an increase in swirl angle (due to an increase in angle of attack or aspect ratio) causes an earlier breakdown. The present experiments in unsteady freestream show that the maximum swirl angle is not correlated with the movement of the vortex breakdown. It is obvious that the variation of the external pressure gradient should be responsible for the dynamic character of the vortex breakdown.

Since dramatic changes take place in the core during the breakdown, its effect on global quantities such as circulation is of primary interest. For this reason, circulation measurements were carried out at each streamwise location (Fig. 4). The dimensionless circulation $\Gamma/U_\infty c$ is shown as a function of streamwise distance and time at the bottom of Fig. 4. The circulation seems to be varying in harmony with the freestream at any x station. It is also an approximately linear function of streamwise distance, except in a region very close to the trailing edge. The circulation in a conical flowfield would also give a linear variation. It is concluded that the variation of circulation is not influenced by the breakdown. This is in agreement with the results obtained for the leading-edge vortex over a steady delta wing.[11]

Conclusions

In this study, the vortex breakdown phenomenon was investigated on a stationary delta wing submerged in an unsteady freestream. Large variations in breakdown location were observed when vortex bursting occurred near the trailing edge. At a certain phase during the acceleration of freestream ($t/T \approx 0.85$), the vortex breakdown suddenly occurs at an upstream location regardless of the angle of attack and the aspect ratio. Around that moment, the axial velocity profile is almost uniform everywhere. After this instant, a wakelike velocity profile is observed.

The maximum swirl angle is almost constant and not correlated with the variations of the vortex breakdown location. This result

suggests that the external pressure gradient might be the cause of the time-dependent nature of the bursting phenomenon.

The circulation around the leading-edge vortex was measured along the vortex axis during the whole cycle. The value of the circulation increases linearly with the distance from the apex and follows the pattern of the variation of the freestream velocity. These variations do not depend on whether the vortex bursting takes place or not. In other words, the vorticity shedding from the leading edge is not affected by the breakdown.

Acknowledgment

This work was supported by a contract from the Air Force Office of Scientific Research.

References

[1]Werle, H., "Sur l'eclatement des tourbillons d'apex d'une aile delta aux fibles vitesses," *La Recherche Aeronautique*, No. 74, Jan.–Feb. 1960, pp. 23–30.

[2]Lambourne, N. C., and Bryer, D. W., "The Bursting of Leading Edge Vortices—Some Observations and Discussion of the Phenomenon," Aeronautical Research Council, R&M 3282, London, 1962.

[3]Wedemeyer, E., "Vortex Breakdown," *High Angle-of-Attack Aerodynamics*, AGARD 121, March 1982.

[4]Lee, M., and Ho, C. M., "Lift Force of Delta Wings," *Applied Mechanics Reviews*, Vol. 43, No. 9, 1990, pp. 209–221.

[5]Rockwell, D., "Three-Dimensional Flow Structure on Delta Wings at High Angle-of-Attack: Experimental Concepts and Issues," AIAA Paper 93-0550, Jan. 1993.

[6]Hall, M. G., "Vortex Breakdown," *Annual Review of Fluid Mechanics*, Vol. 4, 1972, pp. 195–218.

[7]Leibovich, S., "Vortex Stability and Breakdown: Survey and Extension," *AIAA Journal*, Vol. 22, No. 9, 1984, pp. 1192–1206.

[8]Escudier, M., "Vortex Breakdown: Observations and Explanations," *Progress in Aerospace Sciences*, Vol. 25, 1988, pp. 189–229.

[9]Gursul, I., Lin, H., and Ho, C. M., "Vorticity Dynamics of 2-D and 3-D Wings in Unsteady Free Stream," AIAA Paper 91-0010, Jan. 1991.

[10]Gursul, I., and Ho, C. M., "Vortex Breakdown over Delta Wings in Unsteady Free Stream," AIAA Paper 93-0555, Jan. 1993.

[11]Roos, F. W., and Kegelman, J. T., "Recent Explorations of Leading-Edge Vortex Flowfields." NASA High-Angle-of-Attack Technology Conference, NASA Langley Research Center, Hampton, VA, Oct. 30–Nov. 1, 1990.

Boundary Diffusion Controlled Creep Model in Nanocrystals

Konstantinenicholas P. Kaniaris* and
Constantinos S. Lyrintzis†
San Diego State University,
San Diego, California 92182

Introduction

NANOCRYSTALLINE materials (NCMs) by definition are single or multiphase polycrystals with a crystal size on the order of 1–10 nm. NCMs seem to permit the alloying of components, which results in alloys with properties attractive to the aerospace industry. The research around nanocrystals adds a few more difficulties. There is a smaller size and very random arrangement of atoms. Such uncontrollable characteristics are related to the viscosity model by Herring.[1] In aerospace research much time has been spent on changing the shape of crystals by moving atoms around by diffusion. This research has revolved around polycrystalline creep and specifically the work model by Coble.[2]

The focus of this paper is to improve the creep model accepted today along with its diffusivity parameters. By using both the Coble and Herring models and Coffey's assumptions[3] for grain boundary sources and by adjusting the vacancy concentration gradient, one can derive a more accurate nanocrystalline creep equation.

Received June 15, 1992; revision received June 14, 1993; accepted for pubication June 16, 1993.

*Graduate Research Assistant, Department of Mechanical Engineering.

†Associate Professor, Department of Aerospace Engineering and Engineering Mechanics. Member AIAA.

Background

The diffusional creep was shown by Herring[1] to result from a change in equilibrium stress-vacancy concentration. The change in vacancy concentrations is

$$\Delta C = C_o \sigma \Omega / kT \tag{1}$$

where C_o is defined as the equilibrium vacancy concentration at temperature T in a stress-free crystal; σ is the normal to the boundary local stress; k is constant at temperature T; and Ω is the vacancy volume (usually denoted as $\Omega = a_0^3$).

In tensile tests by Nieman et al.,[4] when comparisons between nanocrystalline lead (Pb) and coarse grained Pb were made, the former exhibited an increase in hardness and a significant flaw size sensitivity. Once uniaxial tensile stress is applied, the maximum change in vacancy concentration ΔC occurs on boundaries perpendicular to the applied stress. When boundaries are parallel to stress then the equilibrium vacancy concentration is C_o.

Coble, making some assumptions about the vacancy source on a spherical surface, introduced the boundary diffusion creep rate as

$$\dot{e} = 150\, \sigma D_b W \Omega / (GS)^3\, kT \tag{2}$$

where D_b is the boundary diffusion coefficient, W is the boundary width, and GS is the average grain size. The grain size dependence and the numerical constant differ from Herring's assumptions.

Possibilities for crystal size enhancement were shown by Birringer[5] where grain boundary diffusivity D for a 8-nm crystal was enhanced by a factor of 10^{19} when compared with the lattice diffusion. Such enhancement may be the result of low impurity concentration in the nanocrystalline boundaries as opposed to that of common polycrystals; it could also be rapid diffusion that moves along the connected boundary triple junctions. The earlier enhancement could be the result of the different boundary structures than those of polycrystals.

In the grain's geometry, two restrictions apply. The stress distribution must vary continuously, and the nanocrystalline matrix must continue to expand. As shown in Fig. 1, the atoms relax from the ideal lattice sites given by a hard-sphere model.[5] The relaxation

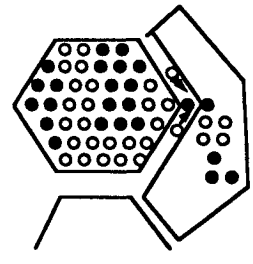

Fig. 1 Nanocrystalline cross section. Different interatomic spacings are shown with arrows.

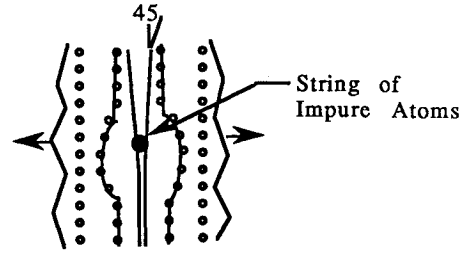

Fig. 2 Boundary interface between slightly tilted crystal grains with primitive lattice structure. The string of impurity is perpendicular to the plane of the figure.